SCIENTIFIC REPORTS

OPEN

Correspondence and
requests for materials
should be addressed to
X.H.L. (cexhli@scut.
edu.cn) or Z.J. (z.
jiang@soton.ac.uk)

Ship-in-a-bottle synthesis of amine-functionalized ionic liquids in NaY zeolite for CO_2 capture

Yinghao Yu[1], Jingzhang Mai[1], Lefu Wang[1], Xuehui Li[1], Zheng Jiang[2] & Furong Wang[1]

[1]School of Chemistry and Chemical Engineering, Pulp & Paper Engineering State Key Laboratory of China, South China University of Technology, Guangzhou 510640, P. R. China, [2]Faculty of Engineering and the Environment, University of Southampton, Highfield, Southampton SO17 1BJ, UK.

CO_2 capture on solid materials possesses significant advantages on the operation cost, process for large-scale CO_2 capture and storage (CCS) that stimulates great interest in exploring high-performance solid CO_2 adsorbents. A ship-in-a-bottle strategy was successfully developed to prepare the [APMIM]Br@NaY host–guest system in which an amine-functionalized ionic liquid (IL), 1-aminopropyl-3-methylimidazolium bromide ([APMIM]Br), was *in-situ* encapsulated in the NaY supercages. The genuine host-guest systems were thoroughly characterized and tested in CO_2 capture from simulated flue gas. It was evidenced the encapsulated ILs are more stable than the bulk ILs. These host–guest systems exhibited superb overall CO_2 capture capacity up to 4.94 mmol g^{-1} and the chemically adsorbed CO_2 achieved 1.85 mmol g^{-1} depending on the [APMIM]Br loading amount. The chemisorbed CO_2 can be desorbed rapidly by flushing with N_2 gas at 50°C. The optimized [APMIM]Br@NaY system remains its original CO_2 capture capacity in multiple cycling tests under prolonged harsh adsorption-desorption conditions. The excellent physicochemical properties and the CO_2 capture performance of the host-guest systems offer them great promise for the future practice in the industrial CO_2 capture.

T he human society is facing unprecedented threat of climate change due to the continuously increasing air CO_2 level induced by the roaring energy demand that will still have to be supplied by fossil fuels in the next decades[1,2]. It was reported the emission of the anthropogenic CO_2 will reach 43 gigatons in 2035, rising 50% from that in 2009[3]. In combating climate change, CO_2 capture and storage (CCS) using various CO_2 absorbents represents the sole effective solution to reduce such a huge scale of CO_2[4]. Currently, organic amines, ionic liquids (ILs) or alkaline scrubbers have been explored as effective absorbents in CCS though they are either corrosive or costly that challenges the process engineering and transportation. Porous solid adsorbents have recently been emerged for CO_2 capture and attracted intensive interest since the materials are less corrosive, cost-effective and easy to transport[5].

To date, various adsorbent materials have been explored for CO_2 capture, including "molecular basket" sorbents (MBS), metal–organic frameworks (MOFs) and alkanolamine modified zeolites[6]. Song and co-workers have done pioneering and systematic research on CO_2 capture with the "molecular basket" sorbents (MBS) and reach the CO_2 adsorption capacity above 3 mmol/g at 75°C and a CO_2 partial pressure of 15 kPa. The MBS materials are featured with the amine polymer (polyethyleneimine, PEI) immobilized onto porous supports (MCM-41[7], SBA-15[8,9], carbon materials[10], bentonite[11], and silica-gel[12]). MOFs have been widely used in gas adsorption due to their unique structural properties, such as robustness, good thermal stabilities and ultrahigh specific surface area[6,13–16] and they can achieve high CO_2 adsorption capacity up to 54 mmol/g under room temperature and high pressure (50 bar)[13]. However, the CO_2 storage capacity of MOFs becomes lower than zeolites at low pressures (<10 bar), not mention that the partial pressure of CO_2 in flue gas is only 0.15 bar[17]. Moreover, MOFs materials suffer from long-term stability issues because the acidic or polar impurities (e.g. H_2S, SO_2, and NO_x, etc) in the flue gas would markedly reduce their CO_2 storage capacity or even damage the structure of MOFs[5]. Commercialized zeolites are more plausible for gas adsorption due to their advantages in large gas uptake at low pressure, high chemical and thermal stability, easier regeneration and moderate cost[18–20]. However, adsorption capacities of zeolites decline rapidly once the temperature is higher than 30°C and even become negligible above 200°C[21]. In addition, their selectivity to CO_2 in the existence of other gases (N_2, CH_4, H_2O, etc.) is not ideal. Hence, the zeolites should be modified for CO_2 capture from flue gas[4,22]. Alkanolamines, such as

Table 1 | Elemental analysis of NaY, [APMIM]Br@NaY-X and [BMIM]Br@NaY

Samples	C (wt %)	H (wt %)	N (wt %)	IL loading (wt %)	IL/supercage
NaY	0.02	2.95	0.25	--	--
[APMIM]Br@NaY-0.5	2.55	2.67	1.45	6.64	0.49
[APMIM]Br@NaY-1	4.35	2.80	2.34	11.36	0.89
[APMIM]Br@NaY-2	6.77	2.74	3.55	17.68	1.49
[APMIM]Br@NaY-4	7.43	2.87	3.73	19.42	1.67
[APMIM]Br@NaY-8	7.62	2.70	4.02	19.92	1.73
[APMIM]Br@NaY-10	8.06	2.69	4.13	**21.06**[a]	1.85
[BMIM]Br@NaY	8.12	1.91	3.11	**18.50**[a]	1.58

[a]In accordance with the results of TGA.

monoethanolamine[23], diethanolamine[24], and tetraethylenepenta-mine[25], have ever been deposited on the zeolites to enhance their selectivity and chemical adsorption capacity of CO_2. However, the alkanolamine are prone to degradation during the regeneration because they are volatile and their amine group are thermal instable. In contrast, owing to the excellent CO_2 capture capacity and physico-chemical properties (negligible vapour pressure, high chemical and thermal stability) of amine-functionalized ILs, they could be poten-tial alternatives for alkanolamines to sort out the selectivity/stability dilemma on the modified zeolite adsorbents, whereas the successful modification must overcome the steric effects arisen from the large molecule sizes of ILs in loading ILs into zeolites[26,27].

Herein, amine-functionalized ILs were encapsulated in the super-cages of zeolite via ship-in-a-bottle strategy[28,29]. In principle, the small precursors of ILs were allowed to diffuse through the zeolite pore apertures and react inside the supercages of zeolite (host), lead-ing to *in-situ* generation of larger IL products (guest) that were entrapped inside the cavities[28,29]. In the present work, with careful consideration of the sizes of precursors, IL candidates, and zeolite supercages[30,31], NaY zeolite and [APMIM]Br were reasonably chosen as the host and the guest, respectively. In order to investigate the effects of IL encapsulation and the properties of the resultants, the obtained [APMIM]Br@NaY host-guest systems with varying load-ing of [APMIM]Br IL were thoroughly characterized through ele-mental analysis, TEM, TGA, BET, XRD, FT-Raman techniques. The CO_2 capture capability of the [APMIM]Br@NaY fell in a desirable range from 3.22 to 4.94 mmol g^{-1} on the dependence of IL loading. The adsorption capability remained unchanged after multiple cyc-ling tests under stringent conditions since the encapsulated [APMIM]Br ILs in NaY were found much more stable than their bulk analogues. Moreover, the optimised [APMIM]Br@NaY can chemically adsorb CO_2 up to 1.85 mmol g^{-1}. The excellent perform-ance of the host-guest materials offers them great potential for the CO_2 capture in large scale.

Results

Physicochemical characteristics of the IL@NaY host-guest sys-tems. The detailed preparation process of all the host-guest systems and the corresponding abbreviations of all the samples were presented in the Methods section. During the synthesis process, all the un-reacted reagents and non-encapsulated ILs were removed from the host-guest systems via careful Soxhlet extraction, while the encapsulated IL guests are too large to escape from the zeolite aperture windows yet kept inside the supercages. The results are in agreement with the observation for $(C_6H_5)_3CCl@HY$ zeolite systems[32], in which $(C_6H_5)_3CCl$ was remained in the HY zeolite supercages, while small precursors of CCl_4 and benzene were removed completely by Soxhlet extraction. Elemental analysis was conducted to determine the molar ratio of encapsulated ILs to supercages (IL/supercage) of NaY zeolite and the results were listed in Table 1. The IL/supercage ratio of [APMIM]Br@NaY-0.5 is 0.49, suggesting that 98% (0.49/0.5 = 0.98) of [APMIM]Br IL was

encapsulated in NaY. The IL/supercage ratio is increased from 0.49 to 1.67 as X increasing from 0.5 to 4, whereas the ratio remains less than 2.0 even when X got to 10. The nonlinear change of the IL/supercage value reveals there is a balance between the guest ILs and supercages. Such ratio can't reach 2.0 because the number of perfect supercages is smaller than the theoretical value (0.67 mmol super-cages per gram of NaY[33]) due to the structural defects existing in the NaY zeolite.

The influence of IL loading on the morphology of NaY zeolite was investigated via TEM characterization. The collected TEM images of NaY, [BMIM]Br@NaY, and [APMIM]Br@NaY-X (shown in Fig. S1-8) are almost the same, suggesting the encapsulated ILs won't affect the rigid framework of the NaY zeolite and thus its morphology remains unchanged.

TGA was conducted to study the thermal stability of NaY zeolite, ILs and the host-guest systems. Typical TGA profiles of NaY, [BMIM]Br, [APMIM]Br and typical host-guest systems ([BMIM]Br@NaY and [APMIM]Br@NaY-10), are comparatively shown in Figure 1. Remarkable weight losses of the bulk ILs of [BMIM]Br and [APMIM]Br appear at 260 and 235°C, respectively, suggesting the thermal decomposition of these ILs initiated at such temperature[34]. However, the onset decomposition temperatures (T_d) are enhanced to 369 and 323°C for the encapsulated [BMIM]Br and [APMIM]Br ILs, respectively, revealing the NaY encapsulated ILs are much more stable than their bulk analogues. The enhanced thermal stability of the ILs in the porous host–guest systems can be attributed to the encapsulation effect of zeolite supercages. When heating up to
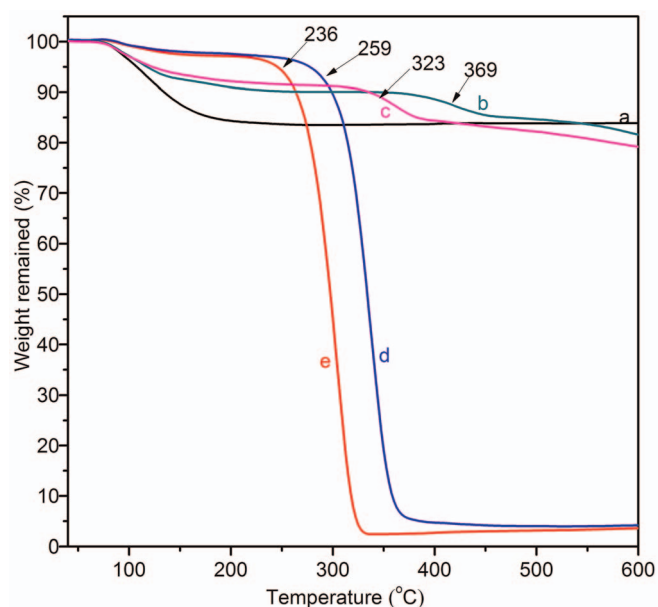

Figure 1 | TGA profiles of (a) NaY, (b) [BMIM]Br@NaY, (c) [APMIM]Br@NaY-10, (d) [BMIM]Br, (e) [APMIM]Br.
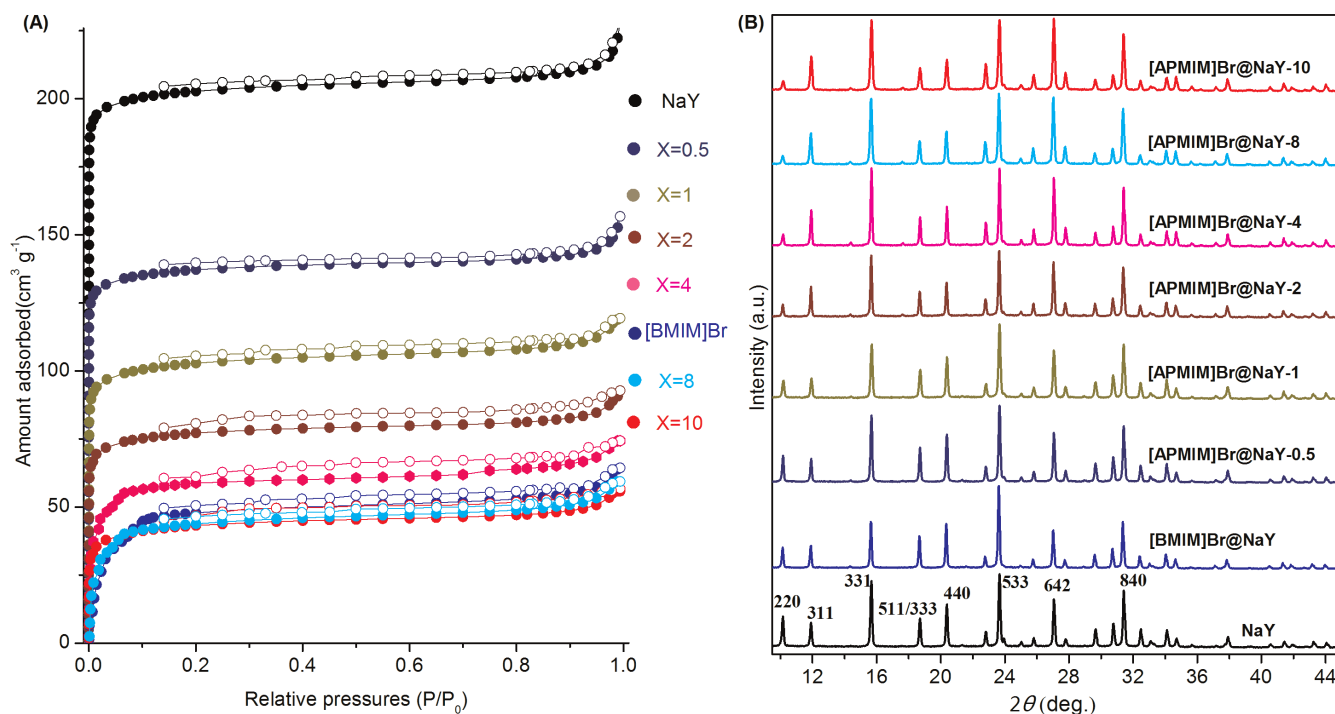
Figure 2 | (A): N$_2$ sorption isotherms (B): XRD spectra of NaY, [BMIM]Br@NaY, and [APMIM]Br@NaY-X (X = 0.5, 1, 2, 4, 8, 10).

600°C, the total weight losses of the [BMIM]Br@NaY and [APMIM]Br@NaY-10 are 18.39 and 20.80%, respectively, which are well consistent with the loading percentages of the corresponding ILs (18.50% of [BMIM]Br and 21.06% of [APMIM]Br as shown in Table 1) on the NaY zeolite. The results verify the ILs have been confined into the pores of the NaY zeolite as discussed in the element analysis.

N$_2$ sorption experiments at −196°C were performed to investigate the surface area of these host-guest systems and the results are shown in Figure 2A. The N$_2$ sorption isotherms of all the samples display typical type-I hysteresis loops along with sharp uptakes in the low relative pressure regions, revealing the characteristic microporous structure of NaY zeolite was not damaged during the fabrication of the host-guest systems. However, the pore volume of the host-guest systems went down nonlinearly as increase of the IL loading, in particular more significant drop when X is smaller than 4. The specific surface areas of the materials were determined using the Brunauer–Emmett–Teller (BET) method to analyze the adsorption branches of the isotherms. As increase the [APMIM]Br loading, the BET specific surface area (S$_{BET}$) of the host-guest materials dropped down from 456 to 149 m^2 g^{-1} which is much smaller than that of NaY (676 m^2 g^{-1}). Such significant drops of S$_{BET}$ also evidenced the ILs had been encapsulated within the NaY supercages rather than loaded on the zeolite external surface.

Figure 2B presents the XRD patterns of NaY and its derived host-guest samples. It can be found that all the samples displayed the similar NaY diffraction patterns, revealing the IL encapsulation process did not destroy the crystalline framework of NaY zeolite, which is in good agreement with the TEM analysis. The close analysis of the XRD patterns shows that the relative diffraction intensities of the NaY [2 2 0] and [3 3 1] Bragg faces (I$_{220}$ and I$_{311}$) varied gradually as increase of the IL loading: I$_{220}$ decreased yet I$_{311}$ increased as more ILs loaded (X value becomes larger). The similar phenomena were ever observed for NaY encapsulating tris(2,2′-bipyridine) ruthenium(II)[35], polypyrrole[36], and sodium bis(trifluoromethanesulfonyl) imide[37]. These phenomena were induced by the larger organic cations driving the randomly-arranged Na$^+$ ions to redistribute into specific sites within the NaY zeolite, in turn, the phenomena further

verify the encapsulation of ILs ([BMIM]Br and [APMIM]Br) into the supercages of NaY zeolite.

Figure 3 shows the FT–Raman spectra of typical samples and Table 2 lists the assignments of the characteristic Raman vibration bands. As shown in Figure 3A, all the host–guest systems ([BMIM]Br@NaY-BE, [BMIM]Br@NaY, [APMIM]Br@NaY-10-BE, and [APMIM]Br@NaY-10) and NaY display the same sharp and characteristic absorption bands around 500 cm^{-1} which are attributed to the framework T–O vibration in NaY zeolite. The results suggest the NaY framework remains during the ship-in-a-bottle synthesis process. Meanwhile, the characteristic Raman vibration bands due to N–CH$_3$ stretching and ring bending (in-plane) at 660 cm^{-1} only show on the genuine N-methylimidazole and [BMIM]Br@NaY-BE and [APMIM]Br@NaY-10-BE samples pre-extraction treatment but disappear from the spectra of [BMIM]Br@NaY and [APMIM]Br@NaY-10 host-guest systems after Soxhlet extraction. The results strongly evidence ILs have been filled into the NaY supercages, in very good accordance with the discussions in TEM, XRD and N$_2$ isotherm sections. The characteristic stretching vibration at 558 cm^{-1} due to C–Br bond in the precursor of 3-bromopropylamine was dismissed for the host–guest systems, which is also related to the specific synthesis strategy. During the ship-in-a-bottle synthesis procedure, N-methylimidazole was initially diffused into the supercages of NaY zeolite following with rapid reaction to generate [APMIM]Br once 3-bromopropylamine added. The as-generated [APMIM]Br would occupy the supercages and thus inhibit further inward diffusion of unreacted 3-bromopropylamine. Hence, unreacted 3-bromopropylamine would be easily removed in the subsequent washing and filtration. In contrast, the pre-entrapped N-methylimidazole molecules were difficult to wash out and necessitated exhaustive Soxhlet extraction. The characteristic Raman shifts of bulk ILs (1023, 1332, 1416, 1453, and 2968 cm^{-1}) remain in the spectra of [BMIM]Br@NaY and [APMIM]Br@NaY-10 even after intensive Soxhlet extraction, clearly revealing that the large-sized [BMIM]Br and [APMIM]Br ILs were encapsulated firmly or sterically confined within the NaY supercages. More importantly, there are no obvious chemical shifts observed between bulk ILs ([BMIM]Br and [APMIM]Br) and their corresponding host-guest systems ([BMIM]

Br@NaY, and [APMIM]Br@NaY-10), indicating there is no covalent bond existing between the immobilized ILs and NaY. The confinement of ILs in the NaY supercages should be mainly attributed to the steric effects and electrostatic forces.

Detailed FT–Raman spectra of [APMIM]Br@NaY-X are shown in Figure 3B. Characteristic bands of ILs at 1023, 1332, and 1416 cm^{-1} can hardly be discerned in the spectrum of [APMIM]Br@NaY-0.5. While the intensities of these bands increase rapidly as the X value increased from 1 to 4. The intensity of the characteristic Raman bands increase slower upon further increasing X value from 8 to 10, suggesting there is an equilibrium for the encapsulation of ILs into the NaY supercages, which also accords well with previous discussions in elemental analysis and XRD sections. In addition, the Raman shifts at 2926 cm^{-1} (CH$_2$ stretching in the side chain) is clearly visible at lower X values but disappears or is merged into the band at 2968 cm^{-1} (CH$_3$ symmetrical stretching) for the high-loading [APMIM]Br@NaY-8 and [APMIM]Br@NaY-10. This can be attributed to unusual changes in the symmetry and coordination geometry of the [APMIM]Br molecules as confined in the NaY supercages[19,38].

CO$_2$ adsorption performance. The CO$_2$ capture capacity of these host-guest systems was evaluated through measurements of their CO$_2$ adsorption isotherms at 0°C from 0 to 1 atm and the results are shown in Figure 4. It can be seen that CO$_2$ adsorption capacity of NaY is 5.89 mmol g^{-1}, and the capacity of [APMIM]Br@NaY-X is decreased from 4.94 to 3.79 mmol g^{-1} with X increasing from 0.5 to 2, and the capacity can still reach up to 3.22 mmol g^{-1} for [APMIM]Br@NaY-10.

The value of the CO$_2$ adsorption comprises of both the chemical and physical adsorption of CO$_2$. As a new class of CO$_2$ adsorbents, it is necessary to investigate the chemisorption performance of the novel host-guest materials since the chemisorbed CO$_2$ is pivotal for CCS. CO$_2$-TPD measurements were carried out to determine the chemisorption amount of CO$_2$ in the host–guest systems

(Figure 5). As shown in Figure 5, all desorption curves were fitted into four characteristic peaks, corresponding to CO$_2$ adsorption on the intrinsic basic sites of NaY (peaks α and β at 180 and 240°C), imidazolium cations (peak γ at 136°C) and –NH$_2$ groups (peak δ at 108°C), which will benefit the analysis of CO$_2$ chemisorption mechanism on both the NaY zeolite and derived host–guest systems. On the NaY zeolite (Figure 5A(a) and 5A(d)), CO$_2$ chemisorbed on the intrinsic Lewis basic sites associated with the lattice oxygen in the NaY framework. In contrast, on the [BMIM]Br@NaY systems (Figure 5A(b) and 5A(e)), CO$_2$ can be chemically adsorbed on both the intrinsic basic sites in NaY and imidazolium cations of the encapsulated ILs. Indeed, the CO$_2$ can reversibly react with imidazolium cations[44] (or imidazolium-like cations[45]) and generate 1,3-dialkylimidazolium-2-carboxylate compound at relatively low temperature. Such a chemisorption was also confirmed by the isosteric heat of CO$_2$ adsorption on [BMIM]Br@NaY (seen in Figure S9-11), where the high adsorption isosteric heat was due to the chemisorption[46,47] on carbene centres in the imidazolium cations. In addition to the two types of chemisorption associated with the lattice oxygen and carbene centres, [APMIM]Br@NaY materials also possess –NH$_2$ group (Figure 5A(c) and 5A(g)) as an extra chemisorption centre. In principle, the active -NH$_2$ groups can react quantitatively with CO$_2$ at the molar ratio of 2:1[26,27]. In brief, as compared in Figure 5A, CO$_2$ chemically adsorbed on the intrinsic Lewis basic sites of NaY is more difficult to be desorbed than the chemisorbed CO$_2$ on the host–guest systems. The phenomenon can be attributed to the stronger basicity of intrinsic basic sites in NaY than that of imidazolium cations or of –NH$_2$ groups[25,48]. As for the [APMIM]Br@NaY host-guest systems, they possess three types of adsorption centers due to the Lewis basic site of NaY, carbene centers and free –NH$_2$ groups. It can be seen from Figure 5A that the CO$_2$ desorption peaks shift to lower temperature along with the increase of ILs loading, suggesting the contribution of Lewis basic centers decreased significantly yet the contribution of carbene and free –NH$_2$ groups improved. The reduced contribution of Lewis basic sites may be arisen from the
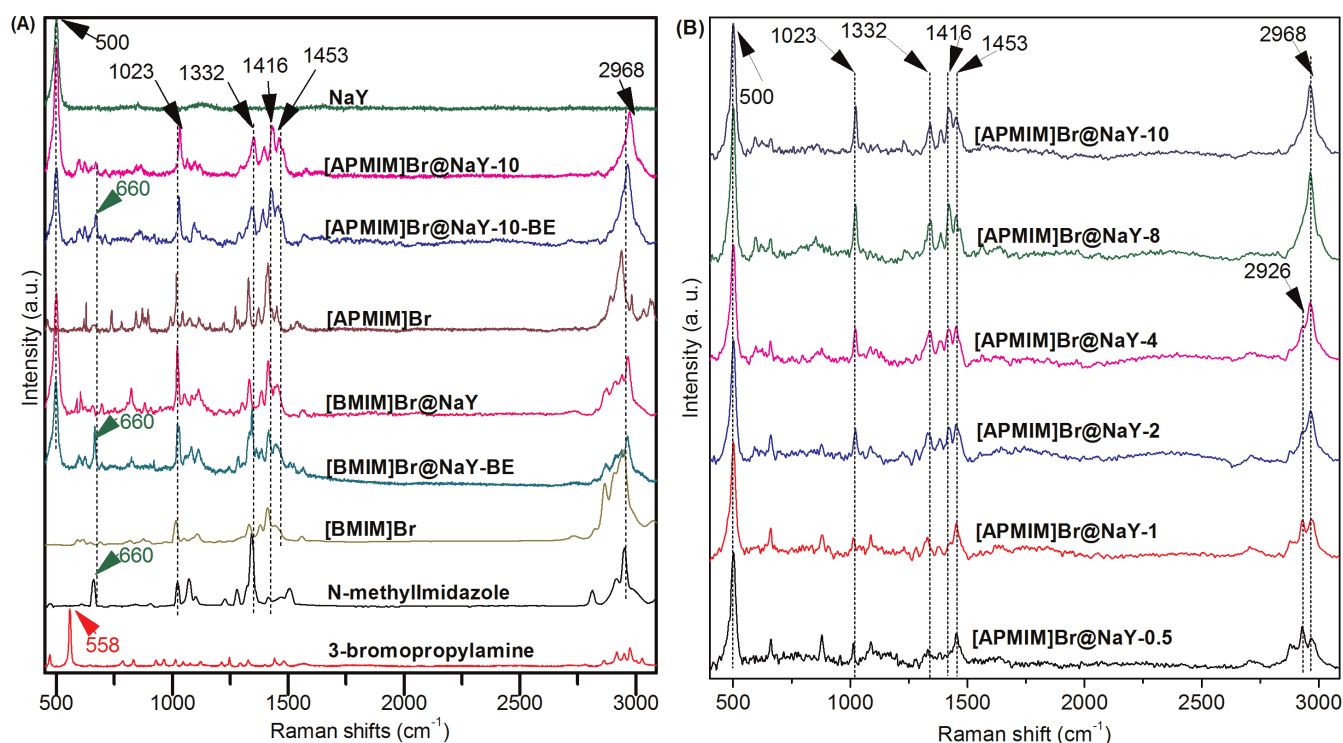

Figure 3 | (A): FT–Raman spectra of N-methylimidazole, 3-bromopropylamine, NaY, [APMIM]Br, [BMIM]Br, [APMIM]Br@NaY-10, [BMIM]Br@NaY, and host–guest systems before Soxhlet extraction ([BMIM]Br@NaY-BE and [APMIM]Br@NaY-10-BE); (B): FT–Raman spectra of [APMIM]Br@NaY-X (X = 0.5, 1, 2, 4, 8, 10).

Table 2 | Characteristic Raman bands and their corresponding assignments

Band (cm^{-1})	Assignments
500	Framework Si–O and Al–O vibration in the zeolite[39]
558	Stretching vibration of C–Br bond in 3-bromopropylamine[40]
660	N–CH$_3$ stretching and ring bending (in-plane)[41]
1023	CH$_3$ bending and ring bending (in-plane)[41,42]
1332	Ring stretching and CH$_3$ bending[41,42]
1416	CH$_3$ symmetrical bending[41,42]
1453	CH$_2$ deformation in the side chain[43]
2926	CH$_2$ stretching in the side chain[43]
2968	CH$_3$ symmetrical stretching in the side chain[43]

ILs coverage on inner walls of NaY pores and the strong interaction between ILs and NaY. The comparison of desorption amount of CO$_2$ adsorbed at 35 and 50°C shows more CO$_2$ was released from the sample adsorbed CO$_2$ at higher temperature, which reveals the ILs functional groups determined the chemisorption of CO$_2$ on the host-guest system. More detailed mechanism of CO$_2$ chemisorption on [APMIM]Br@NaY was proposed in the Supplementary information. From the practical application point of view, the host-guest systems will be easier to regenerate than NaY zeolite as well as more energy-effective for the large scale CO$_2$ adsorption-desorption cycling.

In order to quantitatively investigate the influence of adsorption temperature on the CO$_2$ chemisorption behavior on host-guest materials, their CO$_2$ chemisorption capacities were calculated and listed in Table S1. The area of peak δ in the CO$_2$–TPD profile of [APMIM]Br@NaY-10 is doubled when the adsorption temperature increases from 35 (A=713, Table S1, run c) to 50°C (A=1413, Table S1, run g), while the corresponding CO$_2$ chemisorption capacity increases from 1.38 to 1.85 mmol g^{-1}. The results suggest that the chemisorption induced by –NH$_2$ of the ILs dominated the CO$_2$ chemisorption at relatively high temperature and the interaction between CO$_2$ and –NH$_2$ could be activated by mild heating. More importantly, as shown in Figure 5A(f), upon flushing with N$_2$ at 50°C the peak δ disappears and the amount of the desorbed CO$_2$ decreases from 1.85 mmol g^{-1} (Table S1, run g) to 0.89 mmol/g (Table S1, run f), revealing that CO$_2$ chemisorbed by –NH$_2$ groups can be easily released and this host–guest system of [APMIM]Br@NaY-10 can be regenerated at mild temperature. Low temperature regeneration is highly plausible for practical CCS due to reduced energy penalty.

Figure 5B presents the CO$_2$ desorption profiles on a series of [APMIM]Br@NaY-X and the corresponding desorption areas were calculated (Table S2). CO$_2$ chemisorption capacities of [APMIM]Br@NaY-X increase gradually from 0.98 to 1.85 mmol g^{-1} when X increases from 0.5 to 10. With increasing the IL loading in the host-guest materials, the areas of γ and δ desorption peaks increase sharply (from 335 to 897 and from 0 to 1418, respectively), whereas those of α and β peaks decrease gradually. These changes reveal that the quantities of imidazolium cations (peak γ) and –NH$_2$ groups (peak δ) in the host–guest systems are increased while the number of free Lewis basic sites in the NaY zeolite framework are reduced.

CO$_2$ adsorption capacity in prolonged cycling tests. The adsorption capacity of CO$_2$ on [APMIM]Br@NaY-10 was evaluated in prolonged cycling tests, typically 10 CO$_2$ adsorption-desorption cycles. The structures of the fresh [APMIM]Br@NaY-10 and the recycled sample after 10 cycles of CO$_2$ adsorption-desorption were characterized by XRD. As shown in Figure 6A, the characteristic diffraction peaks of [APMIM]Br@NaY-10 were well preserved after 10 cycles of adsorption-desorption operations, revealing the [APMIM]Br@NaY-10 host-guest adsorbent possesses excellent thermal and chemical stability even at a high desorption temperature, which is crucial for practical CCS process. The percentage ratio of the
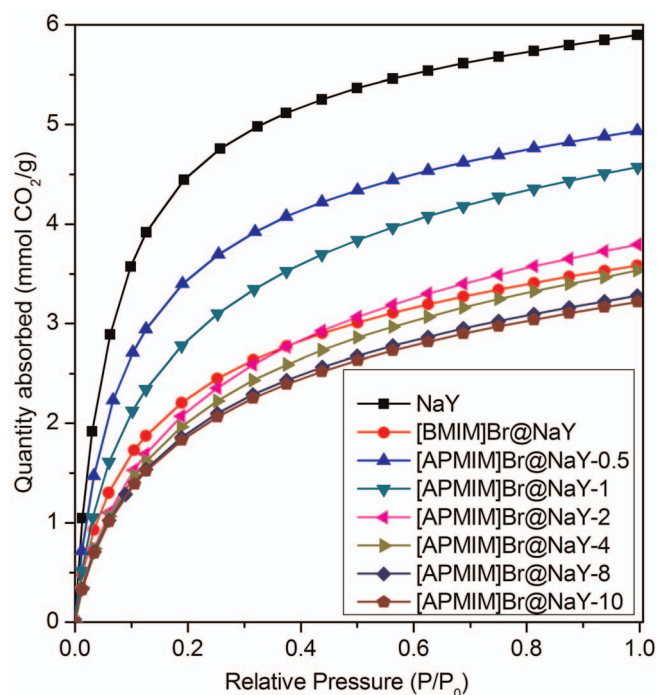

Figure 4 | CO$_2$ adsorption profiles of NaY, [BMIM]Br@NaY, and [APMIM]Br@NaY-X (X = 0.5, 1, 2, 4, 8, 10) at 0°C from 0 to 1 atm.

adsorption capacities of the regenerated to the fresh adsorbent was defined as adsorption index. Figure 6B shows the calculated adsorption indexes in 10 cycling tests of the [APMIM]Br@NaY-10. Clearly, after 10 adsorption-desorption cycling operations the adsorption index was only reduced from 100% to 94.5%, suggesting that most CO$_2$ molecules can be effectively desorbed and the [APMIM]Br@NaY samples are sufficiently stable for recycling applications in CCS process. The negligible decrease of the adsorption capacity can be attributed to the slight loss of accessible −NH$_2$ sites during the high-temperature (280°C) regeneration. As discussed in the CO$_2$ TPD section, CO$_2$ chemisorbed on the [APMIM]Br@NaY can be easily flushed off with N$_2$ at 50°C, hence, the stability of [APMIM]Br@NaY in the harsher prolonged cycling adsorption-desorption tests may promise the material using for the practical CCS.

Discussion

Both zeolites and ILs possess their own remarkable advantages and disadvantages in CO$_2$ capture, while the IL@zeolite host-guest systems would synergistically combine the advantages of individual constituents as well as minimise their disadvantages. Zeolites are featured with high chemical and thermal stability and a moderate cost, but themselves aren't ideal for CO$_2$ capture because of their low adsorption capacity at high temperature and poor selectivity to CO$_2$ over other gases. Indeed, the CO$_2$ adsorption isotherms and TPD results reveal that the CO$_2$ adsorption on NaY is too strong to recover and considerably sensitive to both reaction temperature and pressure. ILs may have high CO$_2$ storage capacity yet is not stable at high temperature as well as necessitate remarkable energy for CO$_2$ capture and regeneration cycles[49]. In the current work, the [APMIM]Br@NaY host-guest systems were successfully synthesised through a facile *in-situ* ship-in-a-bottle synthesis strategy that realised filling a ship (large-sized ILs) into a bottle (NaY microporous supercages). The obtained [APMIM]Br@NaY host-guest systems exhibited superior performance in CO$_2$ capture to the [APMIM]Br IL and NaY zeolite: first, the encapsulated ILs (T_d=323°C) are thermally more stable than the bulk analogues (T_d=236°C) due to the encapsulation effect as well as the strong interaction between the zeolite

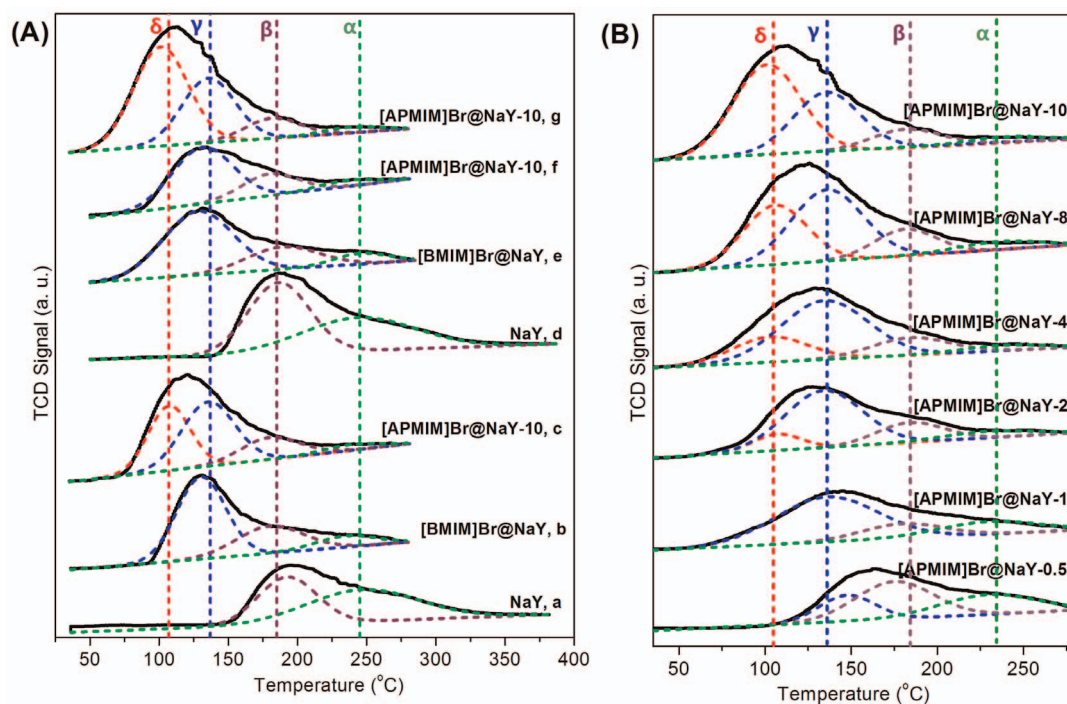**Figure 5** | (A): CO_2 TPD profiles of NaY, [BMIM]Br@NaY, and [APMIM]Br@NaY-10 under various experimental conditions, (a) – (c) CO_2 adsorption at 35°C upon flushing with N_2 at 35°C, (d) – (f) CO_2 adsorption at 50°C upon flushing with N_2 at 50°C, (g) CO_2 adsorption at 50°C upon flushing with N_2 at 35°C; (B): CO_2 TPD profiles of [APMIM]Br@NaY-X (X = 0.5, 1, 2, 4, 8, 10) saturated with CO_2 at 50°C and flushed with N_2 at 35°C.
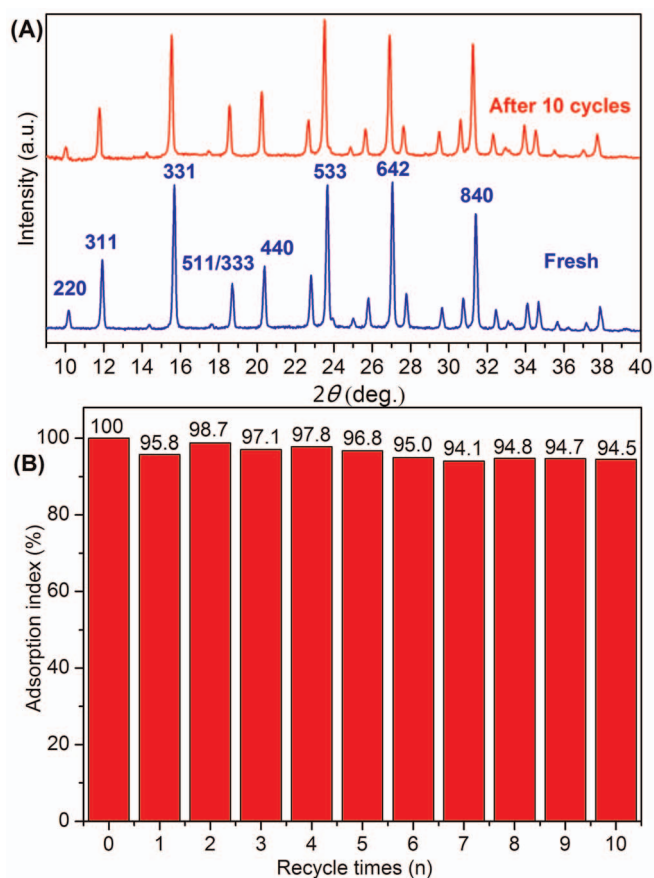

Figure 6 | (A): XRD spectra of [APMIM]Br@NaY-10 (blue: fresh, red: regenerated after 10 cycles); (B): Adsorption indexes of [APMIM]Br@ NaY-10 in 10 cycles.

supercages and ILs; second, at high temperature (50°C), the host-guest system possess higher CO_2 chemisorption capacity than NaY zeolite, which can be attributed to the introduction of imidazolium cations and functional $-NH_2$ groups; third, as shown in CO_2 TPD tests, CO_2 adsorption on [APMIM]Br@NaY is mainly attributed to chemical adsorption that is rather stable during storage and transportation, more importantly, such chemisorbed CO_2 can be easily desorbed by flushing with N_2 at 50°C and thus significantly reduce the energy penalty for the regeneration. The outstanding adsorption-desorption performance of the host-guest systems was verified through the 10 adsorption-regeneration cycling tests under even more stringent conditions. The CO_2 chemisorption capacity of [APMIM]Br@NaY can also be tuned through changing the loading of [APMIM]Br or increasing the functional groups (carbene or $-NH_2$ groups) within ILs. In all, the ship-in-a-bottle synthesis provides a facile strategy to design the IL@zeolite host-guest systems that offer great promise to capture CO_2 from flue gas at large scale and reduced energy penalty.

Methods

Preparation of the host-guest systems. The host-guest systems were prepared by ship-in-a-bottle strategy. The principle of the ship-in-a-bottle synthesis of [APMIM]Br@NaY was presented in Supplementary information and depicted in Figure S13. As shown in Figure S13, N-methylimidazole and 3-bromopropylamine entered supercages of NaY in sequence following with fast reaction with each other to generate [APMIM]Br@NaY. For comparison, the non-alkaline functionalized IL, 1-butyl-3-methyl imidazolium bromide ([BMIM]Br), was also encapsulated in NaY by using the same strategy to obtain [BMIM]Br@NaY. The preparation procedures are detailed as follows.

A series of [APMIM]Br@NaY host–guest systems with varying [APMIM]Br loading amount were prepared by changing the molar ratio of N-methylimidazole to NaY supercages (the molar ratio is abbreviated as X, and the host-guest systems are denoted as [APMIM]Br@NaY-X, X = 0.5, 1, 2, 4, 8, 10). For example, to prepare [APMIM]Br@NaY-8, 3.00 g NaY (~2.00 mmol of supercages[33]) and 1.31 g (16.00 mmol) of N-methylimidazole were added to a flask (50 mL) containing 10 mL ethanol under rigorous stirring at room temperature and N_2 atmosphere for 24 h. 2.43 g 3-bromopropylamine (17.60 mmol), dissolved in 10 mL ethanol) was then added to the mixture and refluxed for another 24 h. The obtained mixture was washed and filtered with ethanol (3 × 20 mL) prior to Soxhlet extraction in ethanol for 24 h. The product was then dried at 80°C in vacuum for 24 h to get a white solid

powder which is [APMIM]Br@NaY-8. [BMIM]Br@NaY was prepared by following the same process with NaY (3.00 g, ~2.00 mmol of supercages), N-methylimidazole (0.82 g, 10.00 mmol), and 1-bromobutane (1.36 g, 11.00 mmol) as starting materials.

Characterization of the host-guest systems. Elemental analysis was performed on a Vario EL III (Elementar). TEM analyses were carried out on a JEOL JEM3010 operated at an acceleration voltage of 300 kV. TGA of samples in N_2 atmosphere from 40 to 600°C was carried out on an STA 449C (Netzsch) at a heating rate of 10°C min^{-1}. Nitrogen sorption isotherms were obtained on an ASAP-2020 (Micromeritics) at −196°C. The samples were degassed at 100°C under vacuum for 6 h prior to adsorption. The Brunauer–Emmett–Teller (BET) theory was used to calculate the specific surface areas. XRD patterns between 5° and 45° were obtained on a Bruker D-8 Advance diffracto-meter equipped with a LynxEye position-sensitive detector and a Cu Kα X-ray source (40 kV, 40 mA) at a scanning step of 0.02°. FT–Raman spectroscopy was carried out by using LabRamHR (Horiba Jobin Yvoc Inc.).

CO_2 adsorption experiments. CO_2 adsorption isotherms under static conditions were recorded on ASAP 2010 (Micromeritics) at 0°C within a pressure range from 0 to 1 atm. Before the adsorption measurements, the samples were degassed via the similar procedure using in BET tests. CO_2 TPD measurements were carried out to determine the amount of the chemisorbed CO_2 using column reactor packed with 0.10 g of adsorbent. The adsorbent was first pre-treated at 200°C for 30 min under 30 mL min^{-1} N_2 flow then cooled to the desired temperature (35 or 50°C) before saturated with CO_2 for 0.5 h. The CO_2 saturated samples were flushed with N_2 gas for 1.0 h to fully remove physically adsorbed CO_2. TPD program was then initiated by heating from the specific adsorption temperature (35 or 50°C) to 380°C (for NaY) or 280°C (for all the host–guest systems) at a rate of 10°C min^{-1}. The amount of desorbed CO_2 should be equal to the amount of CO_2 chemically adsorbed on the sample. The stability of the [APMIM]Br@NaY-10 for CO_2 adsorption was examined in 10 cycles of adsorption-regeneration under the above harsher conditions (adsorption at 50°C and regeneration at 280°C as same as in the TPD experiment) than practical CO_2 capture process.

1. Schiermeier, Q. Putting the carbon back: The hundred billion tonne challenge. *Nature* **442**, 620–623 (2006).
2. Matter, J. M. & Kelemen, P. B. Permanent storage of carbon dioxide in geological reservoirs by mineral carbonation. *Nature Geosci.* **2**, 837–841 (2009).
3. Chu, S. & Majumdar, A. Opportunities and challenges for a sustainable energy future. *Nature* **488**, 294–303 (2012).
4. Xiang, S. *et al.* Microporous metal-organic framework with potential for carbon dioxide capture at ambient conditions. *Nat. Commun.* **3**, 954 (2012).
5. Kenarsari, S. D. *et al.* Review of recent advances in carbon dioxide separation and capture. *RSC Adv.* **3**, 22739–22773 (2013).
6. Zhang, D. S. *et al.* Fluorous metal-organic frameworks with enhanced stability and high H_2/CO_2 storage capacities. *Sci. Rep.* **3** (2013).
7. Xu, X., Song, C., Miller, B. G. & Scaroni, A. W. Influence of moisture on CO_2 separation from gas mixture by a nanoporous adsorbent based on polyethylenimine-modified molecular sieve MCM-41. *Ind. Eng. Chem. Res.* **44**, 8113–8119 (2005).
8. Ma, X., Wang, X. & Song, C. "Molecular basket" sorbents for separation of CO_2 and H_2S from various gas streams. *J. Am. Chem. Soc.* **131**, 5777–5783 (2009).
9. Wang, X. *et al.* A solid molecular basket sorbent for CO_2 capture from gas streams with low CO_2 concentration under ambient conditions. *Phys. Chem. Chem. Phys.* **14**, 1485–1492 (2012).
10. Wang, D., Ma, X., Sentorun, C. & Song, C. Development of carbon-based "molecular basket" sorbent for CO_2 capture. *Ind. Eng. Chem. Res.* **51**, 3048–3057 (2012).
11. Wang, W. *et al.* Sulfuric acid modified bentonite as the support of tetraethylenepentamine for CO_2 capture. *Energy Fuels* **27**, 1538–1546 (2013).
12. Zhang, Z., Ma, X., Wang, D., Song, C. & Wang, Y. Development of silica-gel-supported polyethylenimine sorbents for CO_2 capture from flue gas. *AIChE J.* **58**, 2495–2502 (2012).
13. Sarawade, P., Tan, H. & Polshettiwar, V. Shape- and morphology-controlled Sustainable synthesis of Cu, Co, and in metal organic frameworks with high CO_2 capture capacity. *ACS Sustainable Chem. Eng.* **1**, 66–74 (2013).
14. Long, J. R. & Yaghi, O. M. The pervasive chemistry of metal-organic frameworks. *Chem. Soc. Rev.* **38**, 1213–1214 (2009).
15. Furukawa, H. *et al.* Ultrahigh porosity in metal-organic frameworks. *Science* **329**, 424–428 (2010).
16. Liu, Q. *et al.* Adsorption of carbon dioxide by MIL-101(Cr): Regeneration conditions and influence of flue gas contaminants. *Sci. Rep.* **3**, (2013).
17. D'Alessandro, D. M., Smit, B. & Long, J. R. Carbon dioxide capture: Prospects for new materials. *Angew. Chem. Int. Ed.* **49**, 6058–6082 (2010).
18. Akhtar, F., Liu, Q., Hedin, N. & Bergstrom, L. Strong and binder free structured zeolite sorbents with very high CO_2-over-N_2 selectivities and high capacities to adsorb CO_2 rapidly. *Energy Environ. Sci.* **5**, 7664–7673 (2012).
19. Diaz, E., Munoz, E., Vega, A. & Ordonez, S. Enhancement of the CO_2 retention capacity of Y zeolites by Na and Cs treatments: Effect of adsorption temperature and water treatment. *Ind. Eng. Chem. Res.* **47**, 412–418 (2007).
20. Galhotra, P., Navea, J. G., Larsen, S. C. & Grassian, V. H. Carbon dioxide ($C^{16}O_2$ and $C^{18}O_2$) adsorption in zeolite Y materials: effect of cation, adsorbed water and particle size. *Energy Environ. Sci.* **2**, 401–409 (2009).
21. Wang, Q., Luo, J., Zhong, Z. & Borgna, A. CO_2 capture by solid adsorbents and their applications: current status and new trends. *Energy Environ. Sci.* **4**, 42–55 (2011).
22. Goeppert, A., Meth, S., Prakash, G. K. S. & Olah, G. A. Nanostructured silica as a support for regenerable high-capacity organoamine-based CO_2 sorbents. *Energy Environ. Sci.* **3**, 1949–1960 (2010).
23. Su, F. & Lu, C. CO_2 capture from gas stream by zeolite 13X using a dual-column temperature/vacuum swing adsorption. *Energy Environ. Sci.* **5**, 9021–9027 (2012).
24. Sayari, A. *WO Pat. Appl.* 2004 054708 A2 (2004).
25. Carlisle, T. K., Wiesenauer, E. F., Nicodemus, G. D., Gin, D. L. & Noble, R. D. Ideal CO_2/light gas separation performance of poly(vinylimidazolium) membranes and poly(vinylimidazolium)-ionic liquid composite films. *Ind. Eng. Chem. Res.* **52**, 1023–1032 (2012).
26. Bates, E. D., Mayton, R. D., Ntai, I. & Davis, J. H. CO_2 capture by a task-specific ionic liquid. *J. Am. Chem. Soc.* **124**, 926–927 (2002).
27. Gutowski, K. E. & Maginn, E. J. Amine-functionalized task-specific ionic liquids: a mechanistic explanation for the dramatic increase in viscosity upon complexation with CO_2 from molecular simulation. *J. Am. Chem. Soc.* **130**, 14690–14704 (2008).
28. Tanamura, Y. *et al.* Ship-in-a-bottle synthesis of copper phthalocyanine molecules within mesoporous channels of MCM-41 by a chemical vapor deposition method. *Nano. Lett.* **1**, 387–390 (2001).
29. Alvaro, M. *et al.* Ship-in-a-bottle synthesis of a large guest occupying two Y zeolite neighbour supercages: characterization and photocatalytic activity of the encapsulated bipyrylium ion. *ChemPhysChem* **4**, 483–487 (2003).
30. Selvam, T., Machoke, A. & Schwieger, W. Supported ionic liquids on non-porous and porous inorganic materials—A topical review. *Appl. Catal. A-Gen.* **445–446**, 92–101 (2012).
31. Fowkes, A. J., Ibberson, R. M. & Rosseinsky, M. J. Structural characterization of the redox behavior in copper-exchanged sodium zeolite Y by high-resolution powder neutron diffraction. *Chem. Mater.* **14**, 590–602 (2002).
32. Tao, T. & Maciel, G. E. ^{13}C NMR observation of the triphenylmethyl cation imprisoned inside the zeolite HY supercage. *J. Am. Chem. Soc.* **117**, 12889–12890 (1995).
33. Thoret, J., Man, P. P., Ngokoli, P. & Fraissard, J. Solid-state modification of Y zeolites (NaY or LaNaY) by $MnCl_2$ xH_2O: comparison with V_2O_5, MoO_3 and Sb_2O_3. *Micropor. Mesopor. Mat.* **49**, 45–56 (2001).
34. Fredlake, C. P., Crosthwaite, J. M., Hert, D. G., Aki, S. & Brennecke, J. F. Thermophysical properties of imidazolium-based ionic liquids. *J. Chem. Eng. Data* **49**, 954–964 (2004).
35. Quayle, W. H. & Lunsford, J. H. Tris(2,2′-bipyridine)ruthenium(III) in zeolite Y: characterization and reduction on exposure to water. *Inorg. Chem.* **21**, 97–103 (1982).
36. Nakayama, M., Yano, J., Nakaoka, K. & Ogura, K. Spectroscopic studies on the incorporation of polypyrrole into zeolite channels. *Synthetic. Met.* **138**, 419–422 (2003).
37. Ntais, S. *et al.* Preparation and ion transport properties of NaY zeolite–ionic liquid composites. *J. Power Sources* **196**, 2202–2210 (2011).
38. Bara, J. E. *et al.* Gas separations in fluoroalkyl-functionalized room-temperature ionic liquids using supported liquid membranes. *Chem. Eng. J.* **147**, 43–50 (2009).
39. Yu, Y., Xiong, G., Li, C. & Xiao, F. S. Characterization of aluminosilicate zeolites by UV Raman spectroscopy. *Micropor. Mesopor. Mat.* **46**, 23–34 (2001).
40. Patrick, H. *Fourier Transform Raman spectroscopy*, (Ellis Horwood Limited, Chichester, 1991).
41. Carter, D. A. & Pemberton, J. E. Raman spectroscopy and vibrational assignments of 1- and 2-methylimidazole. *J. Raman Spectrosc.* **28**, 939–946 (1997).
42. Yuan, Y. X., Niu, T. C., Xu, M. M., Yao, J. L. & Gu, R. A. Probing the adsorption of methylimidazole at ionic liquids/Cu electrode interface by surface-enhanced Raman scattering spectroscopy. *J. Raman Spectrosc.* **41**, 516–523 (2010).
43. Berg, R. W., Deetlefs, M., Seddon, K. R., Shim, I. & Thompson, J. M. Raman and ab initio studies of simple and binary 1-alkyl-3-methylimidazolium ionic liquids. *J. Phys. Chem. B* **109**, 19018–19025 (2005).
44. Tudose, A., Demonceau, A. & Delaude, L. Imidazol(in)ium-2-carboxylates as N-heterocyclic carbene precursors in ruthenium–arene catalysts for olefin metathesis and cyclopropanation. *J. Organomet. Chem.* **691**, 5356–5365 (2006).
45. Pawar, G. M. *et al.* Ring-opening metathesis polymerization-derived, polymer-bound Cu-catalysts for click-chemistry and hydrosilylation reactions under micellar conditions. *Dalton Trans.* 9043–9051 (2009).
46. Zhao, Z., Li, X. & Li, Z. Adsorption equilibrium and kinetics of p-xylene on chromium-based metal organic framework MIL-101. *Chem. Eng. J.* **173**, 150–157 (2011).
47. Yang, D. A., Cho, H. Y., Kim, J., Yang, S. T. & Ahn, W. S. CO_2 capture and conversion using Mg-MOF-74 prepared by a sonochemical method. *Energy Environ. Sci.* **5**, 6465–6473 (2012).
48. Selva, M. & Fabris, M. The reaction of glycerol carbonate with primary aromatic amines in the presence of Y- and X-faujasites: the synthesis of N-(2,3-

dihydroxy)propyl anilines and the reaction mechanism. *Green Chem.* **11**, 1161–1172 (2009).

49. Gu, Y. & Li, G. Ionic liquids-based catalysis with solids: State of the art. *Adv. Synth. Catal.* **351**, 817–847 (2009).

Acknowledgments

Author contributions

All the study was designed and the article writing was supervised by X.L. and Z.J. The experiment of BET, TEM, XRD analysis, and prolonged use of the samples was carried out by Y.Y., who was also involved in all the data analyses and paper writing. The experiments of ship-in-a-bottle synthesis, elemental analysis, Raman, CO_2 adsorption was constructed by J.M, he also was a part of the drafting. TGA and the corresponding analysis were carried out by L.W. and F.W. All authors discussed the results and commented on the manuscript.

Additional information

Supplementary information accompanies this paper at http://www.nature.com/scientificreports

Competing financial interests: The authors declare no competing financial interests.

How to cite this article: Yu, Y. *et al.* Ship-in-a-bottle synthesis of amine-functionalized ionic liquids in NaY zeolite for CO_2 capture. *Sci. Rep.* **4**, 5997; DOI:10.1038/srep05997 (2014).

Supplementary Information

Ship-in-a-Bottle Synthesis of Amine-Functionalized Ionic Liquids in NaY Zeolite for CO$_2$ Capture

Yinghao Yu,[a] Jingzhang Mai,[a] Lefu Wang,[a] Xuehui Li,[a,*] Zheng Jiang[b,*] Furong Wang[a]

[a] School of Chemistry and Chemical Engineering, Pulp & Paper Engineering State Key Laboratory of China, South China University of Technology, Guangzhou 510640, P. R. China. Fax: +86 20 8711 4707, E-mail: cexhli@scut.edu.cn

[b] Faculty of Engineering and the Environment, University of Southampton, Highfield, Southampton SO17 1BJ, UK. E-mail: z.jiang@soton.ac.uk

Table of contents

1. TEM of NaY and [APMIM]Br@NaY-X

50 nm

Figure S1 TEM of NaY

50 nm

Figure S2 TEM of [BMIM]Br@NaY

50 nm

Figure S3 TEM of [APMIM]Br@NaY-0.5
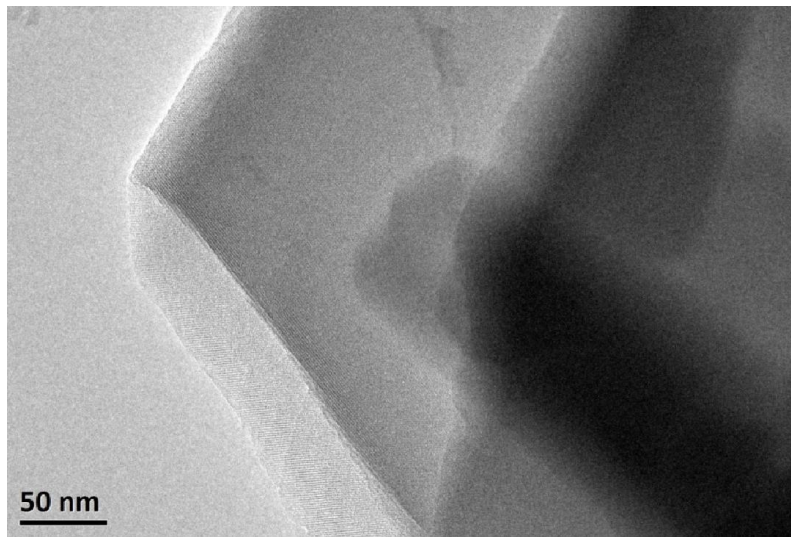
Figure S4 TEM of [APMIM]Br@NaY-1
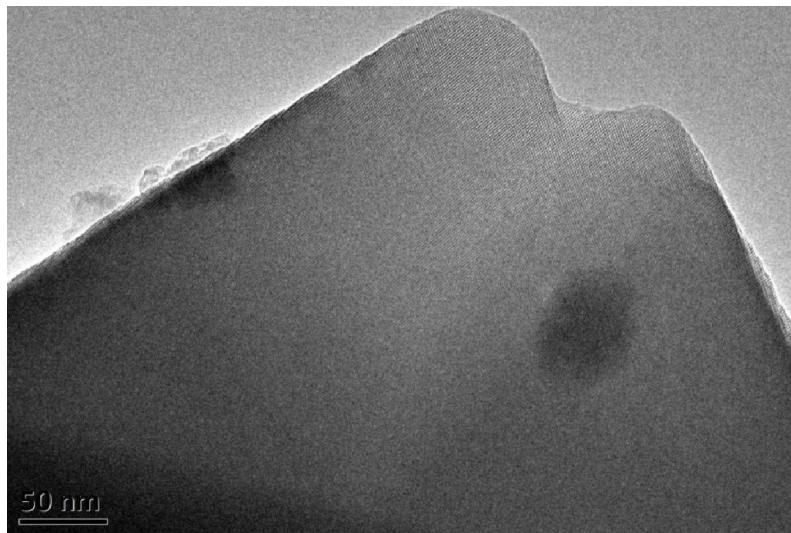
Figure S5 TEM of [APMIM]Br@NaY-2
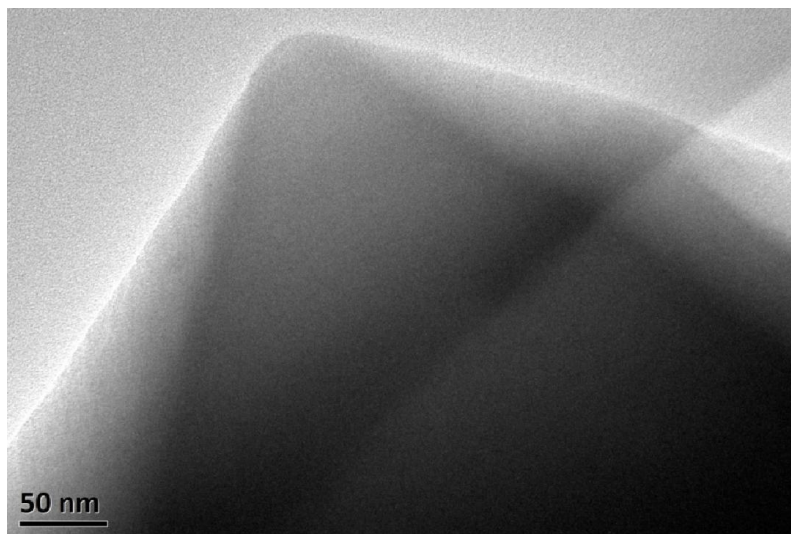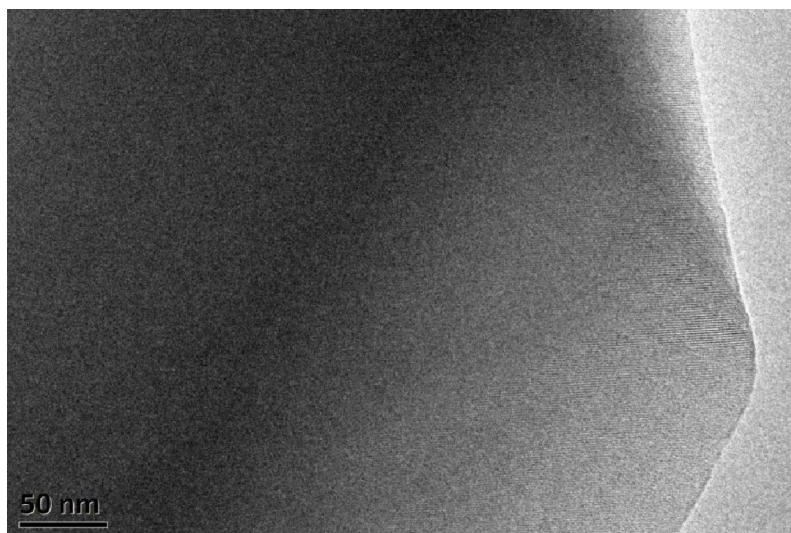

Figure S6 TEM of [APMIM]Br@NaY-4
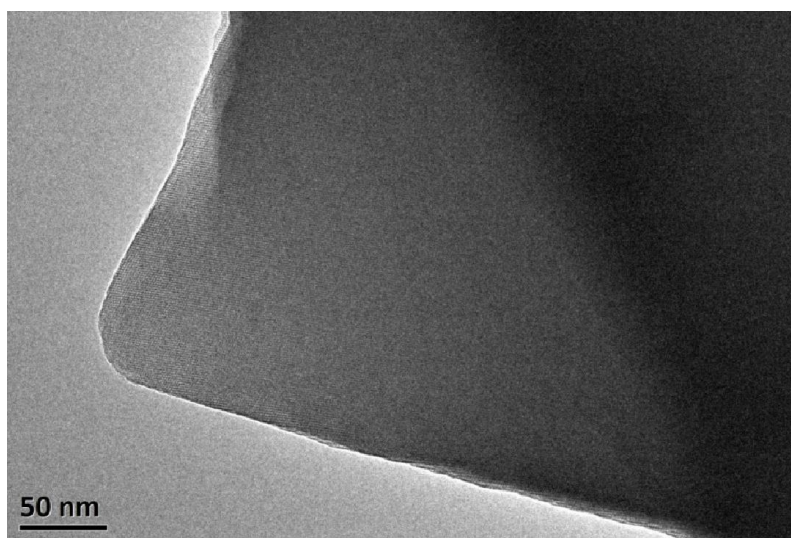
Figure S7 TEM of [APMIM]Br@NaY-8

Figure S8 TEM of [APMIM]Br@NaY-10

2. The isosteric heat of CO_2 sorption on [BMIM]Br@NaY

CO_2 adsorption isotherms of [BMIM]Br@NaY at various temperatures of 283.15, 293.15, 303.15 K had been measured with an Intelligent Gravimetric Analyser (IGA-100, Hiden Analytical Ltd.). Before analysis, the sample (about 20 mg) was degassed in a high vacuum (<0.1 Pa) at 373 K overnight until no further weight losses were observed; the system was then adjusted to the desired temperatures, and the equilibrium data were collected after a stable pressure and weight had been maintained for 90 min at each point to obtain the adsorption isotherm. The experimental adsorption data were fitted to the Langmuir–Freundlich equation, and the isosteric heat of CO_2 adsorption was then calculated by applying the Clausius–Clapeyron equation[1]. The CO_2 adsorption heat curve sharply decreases with CO_2 adsorption amount (from 34 to 22 kJ mol^{-1}). High isosteric adsorption heat at low adsorption amount is due to the active sites in [BMIM]Br@NaY (a carbene center at the 2-position in the imidazolium cations), which contribute strongly towards CO_2 adsorption capacity.

1. Zhao, Z., Li, X. & Li, Z. Adsorption equilibrium and kinetics of p-xylene on chromium-based metal organic framework MIL-101. *Chem. Eng. J.* **173**, 150-157 (2011).
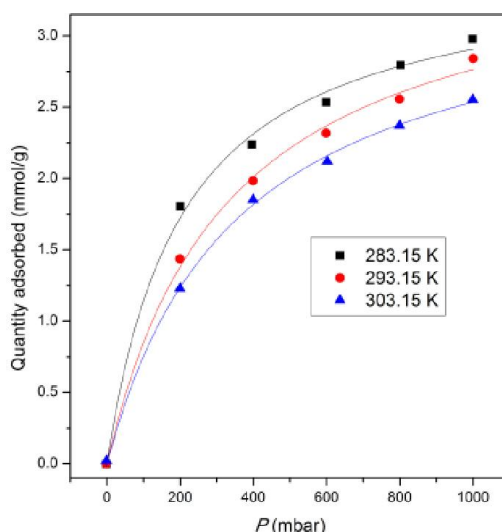
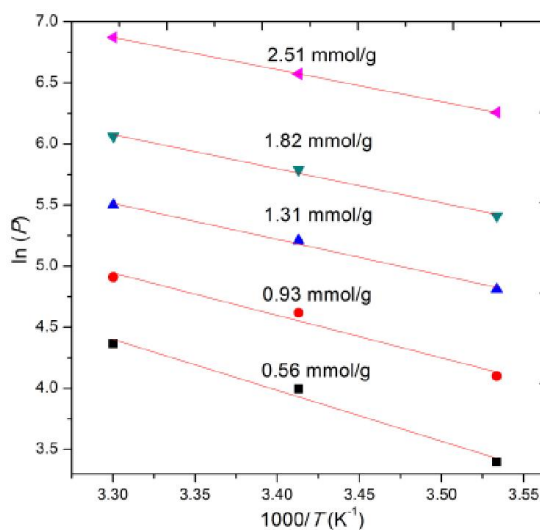Figure S9. Adsorption isotherms of CO_2 on [BMIM]Br@NaY at different temperatures

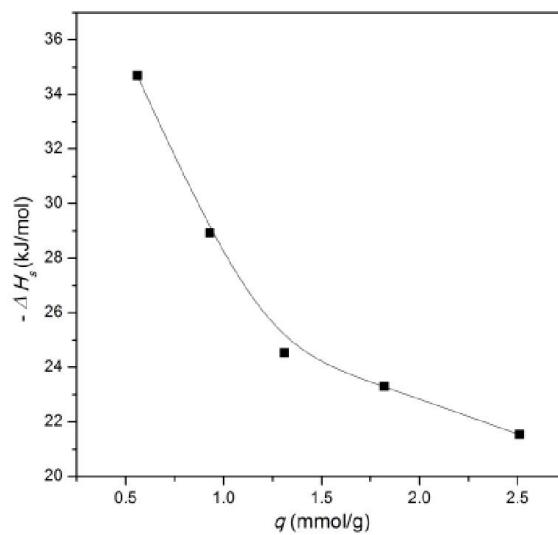Figure S10 Temperature dependence of ln(P) for CO_2 adsorption on [BMIM]Br@NaY

Figure S11 The isosteric heat of CO_2 adsorption as a function of its adsorption amount

3. Table S1 Peak-fitting data for CO_2 TPD experiments on NaY, [BMIM]Br@NaY, and [APMIM]Br@NaY-10

Table S1 Peak-fitting data for CO_2 TPD experiments on NaY, [BMIM]Br@NaY, and [APMIM]Br@NaY-10

Run	Peak α	Peak β	Peak γ	Peak δ	Total area	Desorbed CO_2 [a] (mmol g^{-1} adsorbents) [b]
a	930	730	--	--	1460	0.99
b	174	478	1045	--	1697	1.16
c	81	335	890	713	2019	1.38
d	982	1139	--	--	2121	1.45
e	152	425	1162	--	1739	1.19
f	85	322	899	--	1306	0.89
g	85	291	897	1418	2691	1.85

[a:] The amounts of desorbed CO_2 correspond to the capacities of the materials for chemical adsorption of CO_2. Values were obtained by initial calibration by a series of pulse experiments with known volumes of CO_2, and subsequent calculation using the ideal gas law. [b] Amounts of the adsorbents in all the TPD experiments were fixed at 0.1 g.

4. Table S2 Peak-fitting data for CO$_2$ TPD experiments on [APMIM]Br@NaY-X

Table S2 Peak-fitting data for CO$_2$ TPD experiments on [APMIM]Br@ NaY-X.

X	Peak α	Peak β	Peak γ	Peak δ	Total area	Desorbed CO$_2$ (mmol g^{-1} adsorbent)
0.5	437	668	335	—	1440	0.98
1	295	275	1060	—	1630	1.11
2	131	305	1016	181	1633	1.11
4	103	314	1178	436	2031	1.39
8	154	381	1176	871	2582	1.77
10	85	291	897	1418	2691	1.85

5. The proposed CO_2 chemisorption mechanism of [APMIM]Br@NaY

According to the reported results and our CO_2 TPD study, there exist three types of CO_2 chemisorption in the sample of [APMIM]Br@NaY.

(1): CO_2 can be chemisorbed by the **intrinsic basic sites** in NaY zeolite whereas such basic sites will be partially covered or occupied by [APMIM]Br.

(2): $[APMIM]^+$ cations can also reversibly react with CO_2 to form the compound of 1-aminopropyl-3-methylimidazolium-2-carboxylate.[2,3]

(3): Furthermore, The active sites of $-NH_2$ can react with CO_2 with the molar ratio of 2:1, the proposed CO_2 adsorption pathway of functional groups of $-NH_2$ is explained in Figure S12.[4,5]
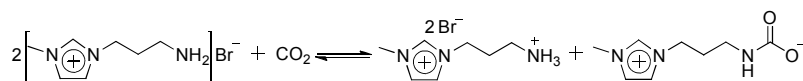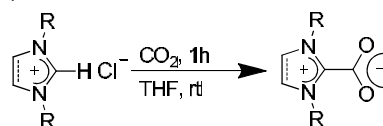

Figure S12 The proposed CO_2 adsorption mechanism of the functional $-NH_2$ group in [APMIM]Br

2. Tudose, A., Demonceau, A. & Delaude, L. Imidazol(in)ium-2-carboxylates as N-heterocyclic carbene precursors in ruthenium–arene catalysts for olefin metathesis and cyclopropanation. *J. Organomet. Chem.* **691**, 5356-5365 (2006).


3. Pawar, G. M., Bantu, B., Weckesser, J., Blechert, S., Wurst, K. & Buchmeiser, M. R. Ring-opening metathesis polymerization-derived, polymer-bound Cu-catalysts for click-chemistry and hydrosilylation reactions under micellar conditions. *Dalton. Trans*. 9043-9051 (2009).
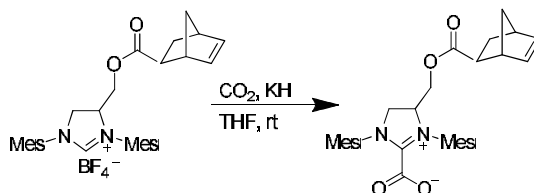
4. Bates, E. D., Mayton, R. D., Ntai, I. & Davis, J. H. CO_2 capture by a task-specific ionic liquid. *J. Am. Chem. Soc.* **124**, 926-927 (2002).
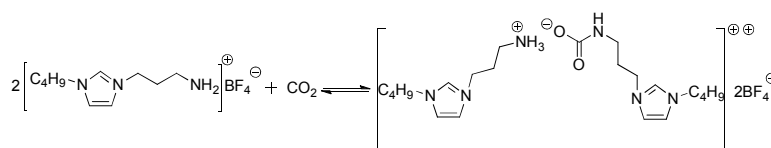
5. Gutowski, K. E. & Maginn, E. J. Amine-functionalized task-specific ionic liquids: a mechanistic explanation for the dramatic increase in viscosity upon complexation with CO_2 from molecular simulation. *J. Am. Chem. Soc.* **130**, 14690-14704 (2008).
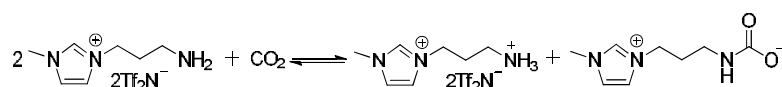
6. The principles of ship in a bottle synthesis of [APMIM]Br@NaY[6]

Some zeolites have a microporous system defining large cavities interconnected by smaller windows. One of the most important examples is NaY, whose internal voids are formed by spherical supercages of 13 Å in diameter, tetrahedrally interconnected through 12-memberedring windows of only 7.4 Å in diameter seen in Figure S13. The smaller precursors (e. g. N-methylimidazole and 3-bromopropylamine) that can diffuse through the zeolite windows and then react inside the supercages to form the target guest ([APMIM]Br), which is allowed to be accommodated inside the cages, however, is too big to cross the windows. So, these guests will remain immobilized by the rigid NaY framework without the possibility of diffusing out of the particle, but they can still interact with small substrates able to diffuse through the micropores (such as CO_2 in this study).
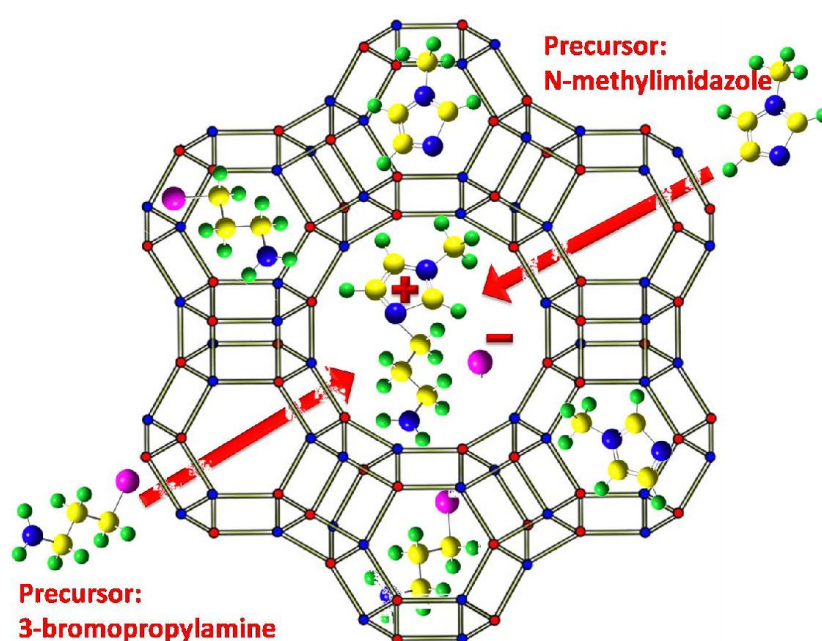

Figure S13 Schematic illustration of ship in a bottle synthesis of [APMIM]Br@NaY

6. Corma A & Garcia H. Supramolecular Host-Guest Systems in Zeolites Prepared by Ship-in-a-Bottle Synthesis. *Eur J Inorg Chem* **2004**, 1143-1164 (2004).